J. Adhesion Sci. Technol., Vol. 14, No. 3, pp. 363–380 (2000)

Characterization of a maleic anhydride-modified polypropylene as an adhesion promoter for glass fiber composites *

G. BOGOEVA-GACEVA [1,†], A. JANEVSKI [1] and E. MÄDER [2]

[1] *Faculty of Technology and Metallurgy, University 'St. Cyril and Methodius', R. Boskovic 16, Skopje, Macedonia*

[2] *Institute of Polymer Research, Hohe Strasse 6, 01069 Dresden, Germany*

Received in final form 20 March 1999

Abstract—Isothermal and nonisothermal crystallizations of isotactic polypropylene (iPP), maleic anhydride (MAH)-grafted PP, and MAH-modified iPP were studied by differential scanning calorimetry (DSC), to evaluate the influence of a small amount of MAH-grafted PP in iPP on its crystallization behavior. Isothermal crystallization was followed in the temperature range from 391 K to 403 K, and the rate constant and Avrami exponents were determined. Nonisothermal crystallization was carried out at different cooling rates (1–20 K/min). It was found that the crystallization kinetics of iPP was significantly altered by modification with the MAH-grafted polymer. A decreased equilibrium melting temperature, as well as decreased surface energy of folding and critical dimensions of a growing nucleus, was determined for the MAH-modified iPP, indicating faster growth of lamellae and a higher rate of crystallization. The improved nucleation ability of the modified polymer was shown to cause a shift in the crystallization peak temperature towards higher values (from 393.7 K to 399.6 K, at a cooling rate of 1 K/min), resulting in crystal structures less disposed to recrystallization. Model composites of iPP and MAH-modified iPP with glass fibers were also analysed. The apparent shear strength of single-fiber model composites with MAH-modified iPP was drastically increased compared with homo-iPP.

Keywords: Isotactic polypropylene; maleinated polypropylene; crystallization; isothermal; nonisothermal; apparent shear strength.

NOTATION

α	crystal conversion
β	cooling rate

*This work is dedicated to the memory of Professor H.-J. Jacobasch.

†To whom correspondence should be addressed. E-mail: gordana@ereb.mf.ukim.edu.mk

t_i	induction time
$t_{0.5}$	half-time of crystallization
γ	constant which represents the ratio between the final thickness of crystalline lamellae and the initial critical thickness
k	rate constant of crystallization
n	Avrami coefficient
T_c	crystallization temperature
T_m°	equilibrium melting temperature
T_m'	observed melting temperature
T_g	glass transition temperature
T_p	temperature at which $d\alpha/dT$ reaches its peak value
T_{hm}	temperature of high melting peak
T_{lm}	temperature of low melting peak
ΔT	supercooling, $\Delta T = T_m^\circ - T_c$
ΔT_p	undercooling at which $d\alpha/dT$ reaches its peak value
ΔT_{mp}	difference between the high (T_{hm}) and low (T_{lm}) melting peaks
A_0	constant
$\Delta\Phi^*$	energy of formation of a nucleus with critical dimensions
σ	crystal growth lateral surface energy
σ_e	crystal fold surface energy
ΔH_f	enthalpy of fusion
ΔH_u	enthalpy of fusion per unit volume
ΔG_u	difference between the free energies for the polymer melt and crystal
R	universal gas constant
K	Boltzmann constant
b_0	molecular thickness
C_1, C_2	constants
l	lamellar thickness
l^*	thickness of the critical crystal secondary nucleus
G	spherulite growth rate, determined from optical microscopy data

1. INTRODUCTION

Isotactic polypropylene (iPP) is a widely used thermoplastic because of its versatility, low cost, and a number of desirable properties. iPP has been studied extensively and its crystallization with numerous inorganic and organic nucleating agents has been reported [1–3], among which talc, sodium benzoate, aluminum benzoate, and

dibenzylidene sorbitol are most frequently used. To tailor their nucleating activity, surface treatments are often carried out [4]. Recently, the application of some polymers as nucleating agents for PP, such as polycyclopentene and polyvinylcyclohexane, has also been examined [5]. Generally, the effect of nucleating agents is judged by the decrease in crystallite size compared with that of the pure polymer and its impact on the material characteristics, such as the modulus and transparency. Used in low concentration, these agents, acting as heterogeneous nuclei, usually increase the rate of isothermal crystallization [3, 6]. During nonisothermal crystallization from the melt, the temperature of crystallization of the nucleated polymer is shifted towards higher temperature [7, 8]. For these reasons, nucleating agents are widely used in industry to reduce processing times and to improve the properties of iPP. Nucleating agents such as quinacridone and a bicomponent mixture consisting of equivalent amounts of pimelic acid and calcium stearate are used to produce different levels of β-form iPP, which, in turn, improves the impact strength of PP [8, 9], an effect related to the difference in spherulite morphologies between the α- and β-crystallites [10, 11].

Recently, the consumption rate of iPP in fiber-reinforced composites has become very high, due to the favorable price/performance ratio and to the development of some new technologies, based on innovative cost-effective composite preforms consisting of reinforcing fibers and thermoplastic filaments or powder [12, 13]. However, due to its nonpolar nature, the use of homo-iPP in composite materials, in which the bonding between the fibers and the polymer matrix strongly affect the overall composite properties, is limited.

Besides the use of nucleating agents capable of altering the crystallization behavior of iPP, different methods of chemical modification of PPs are currently being developed to improve the compatibility with and the adhesion to the reinforcing fibers and to tailor the interface-sensitive properties of composite materials [14].

The chemical modification of iPP through the grafting of different monomers offers the possibility of introducing polar functional groups into the polymer backbone without adversely affecting the basic properties of the polymer. The grafting of acrylic and methacrylic acids, as well as acrylamide, ethylene glycol methacrylate, and maleic anhydride (MAH), has been reported in the literature [15, 16]. Improved adhesion to numerous fillers and decreased critical surface tension were observed for MAH-grafted PP, even at low degrees of grafting [15].

In our previous papers, the results of DSC analyses of the crystallization and melting behavior of iPP in model composites with glass fibers were presented [17, 18]. These investigations were carried out to clarify the role of treatment of the glass fibers on the adhesion phenomena and the related composite properties. It was shown that differently treated or sized glass fibers exhibited different nucleating abilities towards iPP. Further, we investigated the morphology of unmodified and MAH-modified iPP, developed in the Institute of Polymer Research, Dresden, as a matrix material for glass fiber composites [19]. Our investigations, carried out by polarizing optical microscopy, have shown that the presence of MAH-grafted

PP used as a modifier in iPP leads to an alteration of the crystallization kinetics, although a spherulite morphology similar to that in neat iPP was developed [20].

On the basis of the results obtained in this study, we expect the process parameters of the production cycle of glass fiber/PP composites to be tailored so as to obtain a certain polymer morphology and corresponding properties of the composite. In this paper, the crystallization kinetics of MAH-modified iPP is analysed by DSC, and the basic energetic parameters of crystallization are determined and compared with those of homo-iPP and maleinated iPP. To summarize the characteristics of PPs as matrices for glass fiber composites, besides crystallization kinetics data, their adhesion characteristics towards specially sized glass fibers are also given.

2. EXPERIMENTAL

The crystallization behavior of three polypropylenes (PPs) was investigated. Maleic anhydride-modified PP (designated M-PP) with a melting flow index, MFI, of 36 g/10 min was produced from commercial grade Shell homo-iPP (designated PP-S) with a weight-average molecular weight, M_w, of 158 500, as determined by GPC, and a polydispersity index, M_w/M_n, of 6.36; and commercial grade modifier, MAH-grafted PP (Polybond 3150, designated PB) with M_w 90 000, MFI = 50 g/10 min, and a grafting degree of 0.5% MAH.

^{13}C-NMR spectra were recorded at 398 K using a Bruker DRX 500 spectrometer at 500.13 MHz for ^{1}H and 125.77 MHz for ^{13}C. The polymer samples were dissolved in a mixed solvent of 1,2,4-trichlorobenzene and benzene-d_6 (4 : 1 volume ratio). The polymer concentration was 9%. In all measurements, broad-band noise decoupling was used to remove ^{13}C–^{1}H coupling. The pulse repetition was 4 s and 1200 scans were performed (see Table 1).

Isothermal and nonisothermal crystallizations of PPs were analysed by DSC. In the isothermal regime, the sample was rapidly heated to 478 K and held in the molten state for 5 min, to erase the thermal history of the polymer. Then the sample was cooled to a given crystallization temperature (T_c) with a cooling rate of 80 K/min. Isothermal crystallization was carried out at T_c until crystallization was completed. The crystallization under nonisothermal conditions was performed by cooling at different cooling rates: 1, 3, 5, 10, 15, and 20 K/min. The experiments were carried out with a Perkin Elmer DSC-7 analyzer under nitrogen and the calibration was performed with indium and zinc. The sample weight in all experiments was 7.0 mg. Based on the determined values for the enthalpy of crystallization, the extent of crystallization (crystal conversion), α, is calculated as

$$\alpha = \int_0^t (\mathrm{d}H/\mathrm{d}t)\,\mathrm{d}t \Big/ \int_0^\infty (\mathrm{d}H/\mathrm{d}t)\,\mathrm{d}t = f(t). \tag{1}$$

From the $\alpha = f(t)$ curves obtained, the time of induction (t_i) [21] as well as the half-time of crystallization ($t_{0.5}$) was determined.

Single-fiber model composites of glass fibers and polypropylene (PP) matrix were prepared to carry out single-fiber pull-out tests. A self-made pull-out apparatus [19] was used which allows high precision fiber displacement and force measurements on end-embedded fibers. The fibers were embedded at 230°C under an argon atmosphere. The embedding fiber lengths of 10–300 μm were examined. The pull-out test was carried out at identical velocities of pulling out the fibers (0.2 μm/s) at ambient temperature. From each force–displacement curve, the force at debonding, F_d, and the embedded length, l_e, were determined and the apparent interfacial shear strength (IFSS), τ_{app}, calculated using the simple Kelly–Tyson formula $\tau_{app} = F_d/2r_f\pi l_e$, was assumed to be equal to a shear force that was applied to the entire interface and distributed uniformly. The fiber diameter $D = 2r_f$ was measured microscopically. A well compatible sizing for glass fibers consisting of γ-aminopropyl-triethoxysilane and PP film former was used. The model fibers were made in a continuous process of filament spinning and sizing using a unique equipment at the Institute of Polymer Research. About 15–20 single tests were carried out to calculate the mean values of each fiber/polymer combination.

The wetting measurements with test liquids (sessile drop method) were used to characterize the surface energetic behavior in the solid state for the PP matrix. Dynamic wetting measurements on the glass fibers were made using a Krüss K 14 tensiometer. A single fiber was fixed at a sample carrier by means of adhesive tape. A microbalance measured the force applied to the fiber by the liquid as the liquid container was raised and withdrawn. The sensitivity of the microbalance was ± 1 μg. The stage speed was 0.1 mm/min for the tests using doubly distilled and deionized water (measured surface tension = 72.2 mN/m). The fiber perimeter was measured for each continuous filament (filament cut in several pieces of fibers of the same diameter which had been used for wetting with the two liquids) by means of the wetting force at zero depth of immersion of a completely wetting liquid (n-hexane).

The thermodynamic work of adhesion was calculated from the surface free energies of the fibers and the solid polymer matrix was determined by contact angle measurements with water and methylene iodide using the geometric mean equation of Owens and Wendt.

3. THEORETICAL BACKGROUND

From DSC scans (isothermal crystallization at given T_c and then melting of the crystallized sample) the equilibrium melting temperature (T_m^o) was determined by the Hoffman–Weeks method [22]:

$$T_m' = T_m^o(\gamma - 1)/\gamma + T_c/\gamma, \tag{2}$$

where γ is a constant which represents the ratio between the final thickness of the crystalline lamellae and the initial critical thickness, and T_m' is the observed melting temperature of the sample isothermally crystallized at T_c.

According to the kinetic theory of polymer crystallization [23], assuming that the growth of lamellae is controlled by a process of secondary nucleation, the temperature dependence of the crystallization rate, k, is given by the relation

$$\log(k)/n = A_0 - \Delta F^*/2.3RT_c - \Delta\Phi^*/2.3KT_c, \tag{3}$$

where A_0 is a constant (assuming that the primary nucleation density at each T_c examined does not vary with time), ΔF^* is the activation energy for the transport of crystallizing units across the liquid/solid interface, K is the Boltzmann constant, n is the Avrami exponent, and $\Delta\Phi^*$ is the energy of formation of a nucleus with critical dimensions, expressed as [23]

$$\Delta\Phi^* = 4b_0\sigma\sigma_e T_m^o/\Delta H_f \Delta T. \tag{4}$$

In this equation b_0 is the molecular thickness and σ and σ_e are the crystal growth lateral surface energy and the crystal fold surface energy, respectively. ΔH_f is the enthalpy of fusion and $\Delta T = T_m^o - T_c$ is supercooling. ΔF^* is usually expressed as the activation energy of viscous flow given by the Williams–Landel–Ferry relation [24]:

$$\Delta F^* = C_1 T_c/(C_2 + T_c - T_g), \tag{5}$$

where C_1 and C_2 are constants ($C_1 = 17.2$ kJ/mol; $C_2 = 51.5$ K) and T_g is the glass transition temperature. In further calculations, the literature value of $T_g = 260$ K [25] was used.

The plot of $[\log(k)/n + \Delta F^*/2.3RT_c]$ versus $T_m^o/T_c\Delta T$ yields a straight line with a negative slope proportional to

$$4b_0\sigma\sigma_e/2.3K\Delta H_f, \tag{6}$$

from which $\Delta\Phi^*$ and σ_e are obtained assuming that $b_0 = 0.525$ nm [26], $\Delta H_f = 209$ kJ/kg [27], and $\sigma = 0.1b_0\Delta H_f$.

The relation between the lamellar thickness (l) and T_m' is given by the following equation [28]:

$$T_m' = T_m^o[1 - (2\sigma_e/\Delta H_u l)], \tag{7}$$

where ΔH_u is the heat of fusion per unit volume of the polymer with 100% crystallinity ($\Delta H_u = 1.99 \times 10^8$ J/m^3).

The thickness of the crystal critical nucleus is given as [28]:

$$l^* = 2\sigma_e/\Delta G_u, \tag{8}$$

where ΔG_u is the difference between the free energies for the polymer melt and crystal, and can be approximated as $\Delta H_u \Delta T/T_m$.

4. RESULTS AND DISCUSSION

4.1. Isothermal crystallization

On the basis of the DSC scans of isothermal crystallization, crystal conversions were determined and as demonstrated by Fig. 1, the plot of $\log[-\ln(1-\alpha)]$ versus $\log(t)$ yields a straight line. This indicates that the kinetics of crystallization follows the Avrami equation [29, 30]. The rate constant k and the Avrami exponent n were

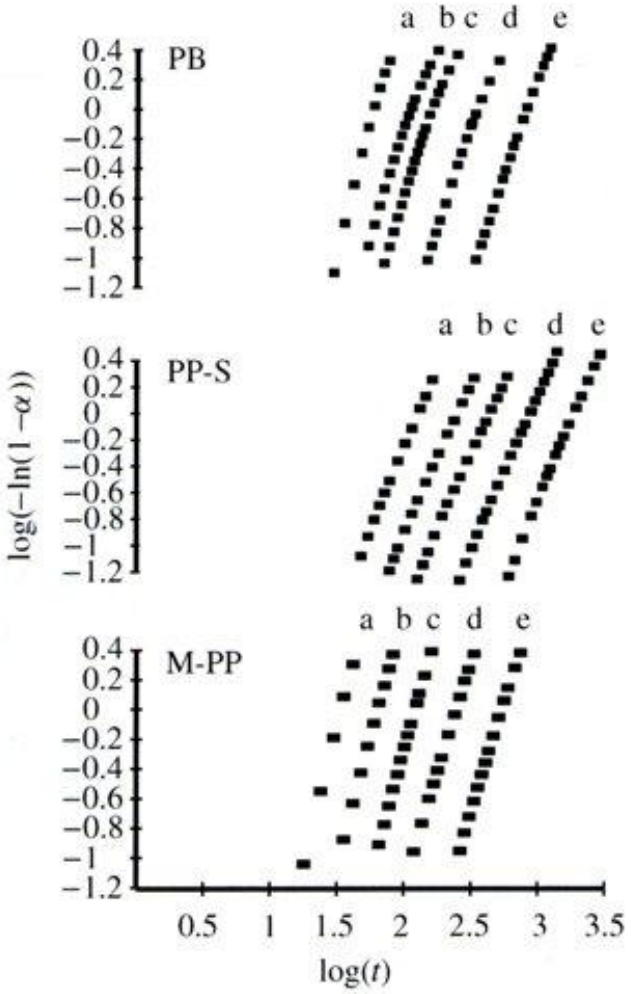

Figure 1. Avrami plots of PB, PP-S, and M-PP at different T_c's (K): (a) 391; (b) 394; (c) 397; (d) 400; (e) 403. t is given in s.

Table 1.
Concentrations of meso triads (*mm*), probabilities for meso additions (P_m), and their average lengths (n)

	PP-S	PB
mm	0.94	0.96
P_m	0.96	0.97
n	23.2	36.3

Table 2.
Avrami index n and kinetic constant k at different T_c values

	PP-S		PB		M-PP	
T_c (K)	n	k	n	k	n	k
391	3.4	7.6×10^{-7}	2.5	6.2×10^{-6}	3.6	2.4×10^{-6}
394	2.6	3.5×10^{-6}	2.3	3.5×10^{-6}	3.4	7.3×10^{-6}
397	2.6	1.3×10^{-6}	2.3	1.1×10^{-6}	3.3	1.2×10^{-7}
400	2.5	3.6×10^{-7}	2.3	1.4×10^{-7}	3.0	7.0×10^{-8}
403	2.6	2.7×10^{-8}	2.4	1.1×10^{-8}	3.0	7.5×10^{-9}

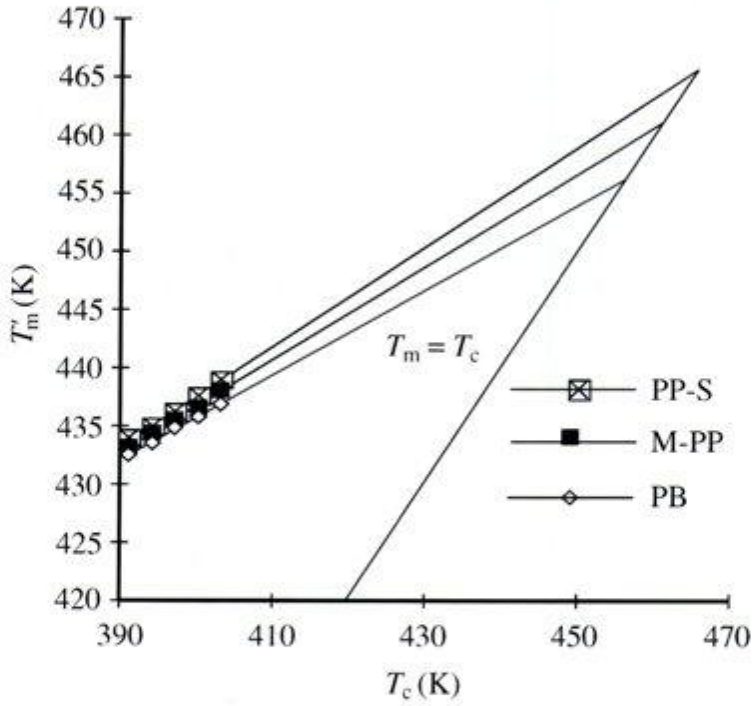

Figure 2. Hoffman–Weeks plot of PP-S, M-PP, and PB.

determined and the results are given in Table 2. Different values for n, ranging from 3.6 to 2.3, were found for the pure iPP (PP-S), PB, and M-PP, with a similar tendency of decreasing n with increasing T_c. This effect was more pronounced for PP-S, pointing out the differences in nucleation mechanisms of these three PPs.

The equilibrium melting temperature was determined by the Hoffman–Weeks method and the results are presented in Fig. 2. Generally, the melting of iPP following crystallization results in the appearance of two melting peaks, related to the reorganization processes in the melting range taking place during the DSC run. However, in the range of crystallization temperatures analysed, in our experiments only one melting peak appeared. The values of the maxima of the melting peaks (T_m') were used for the determination of T_m^o.

As can be seen from Table 3, T_m^o of MAH-modified PP (M-PP) lies between the values of T_m^o for pure PP-S and MAH-grafted PP (PB), being lower than T_m^o

Table 3.
Surface energy of folding, σ_e, equilibrium melting temperature, and γ constant determined from isothermal data

	PP-S	PB	M-PP
σ_e (mJ/m^2)	209	153	187
T_m° (K)	466	456	462
γ	2.3	2.7	2.5

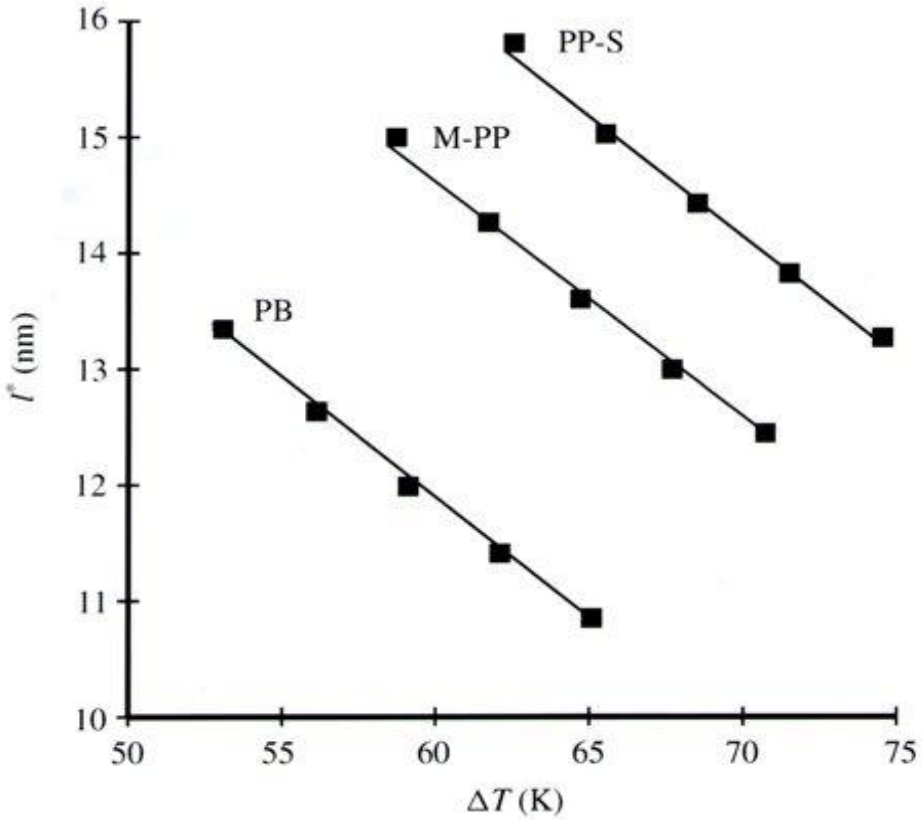

Figure 3. Thickness of the critical nucleus, l^*, versus ΔT.

of PP-S. Relatively high T_m^o values of PPs are characteristic of iPP with a high content of isotactic segments [31], as determined for the examined polymers by NMR (Table 1). The literature values of T_m^o for iPP with a high isotacticity content are between 457.4 [32] and 481 K [33].

The values of the γ constant are also given in Table 3 and it can be seen that the highest value of γ, representing the ratio between the final thickness of the crystalline lamellae and the initial thickness, is found for MAH-grafted PP (PB). The parameters which control the growth of lamellae were determined from the values of T_m^o and the corresponding data obtained from the Avrami plots. The crystal fold surface energy (σ_e) and the critical dimensions of a stable secondary nucleus (l^*) which can grow further were determined. The free energy of the crystal fold

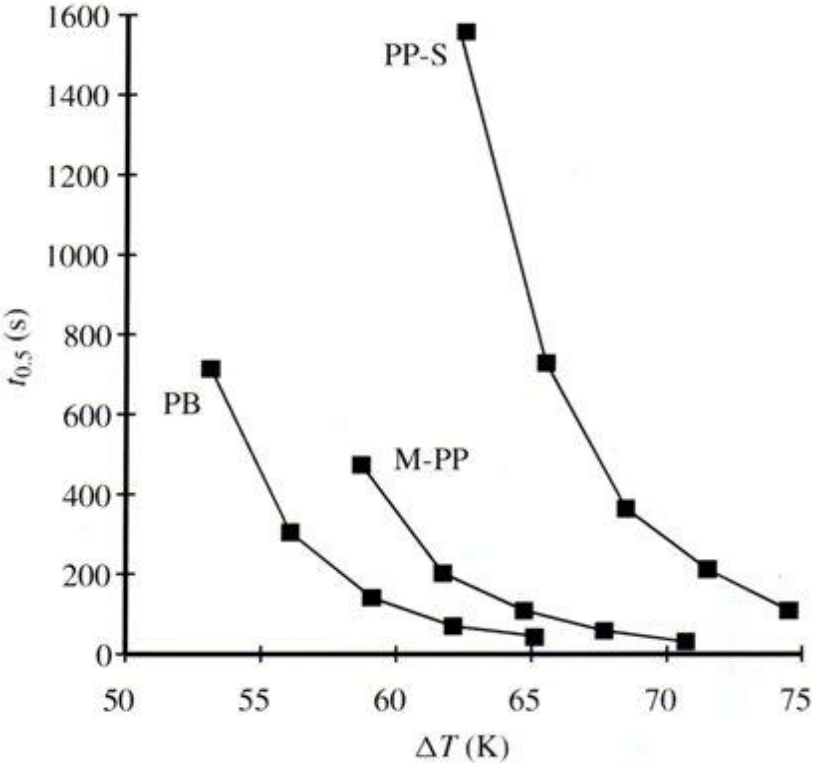

Figure 4. Dependence of $t_{0.5}$ on ΔT for different polymers.

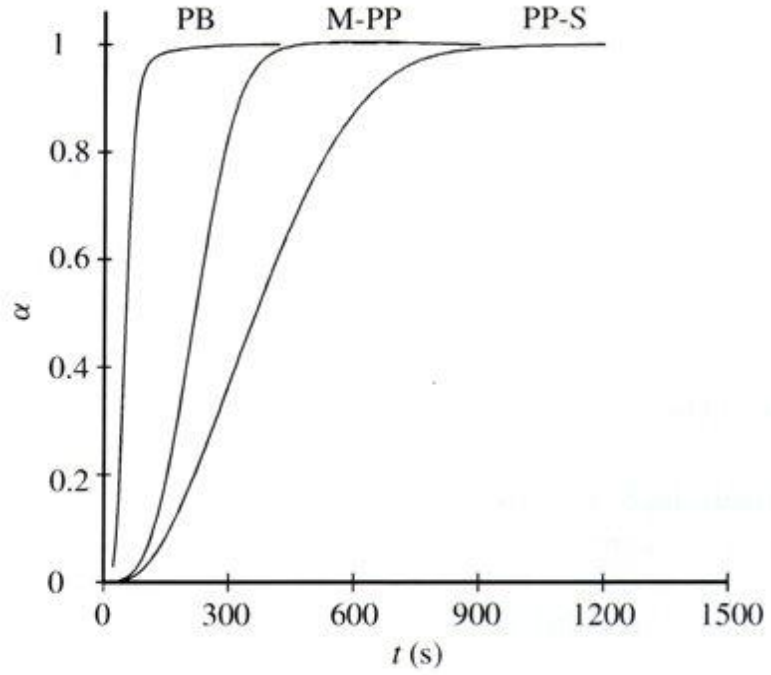

Figure 5. Conversion curves of the polymers at $\Delta T = 65$ K. T_c (K): 400 for PP-S, 391 for PB, and 397 for M-PP.

surface (see Table 3) and the critical dimensions of a growing nucleus (see Fig. 3) both representing a precondition for faster growth of lamellae and a higher rate of crystallization, are lower for PB than for PP-S. This was confirmed by the plot of

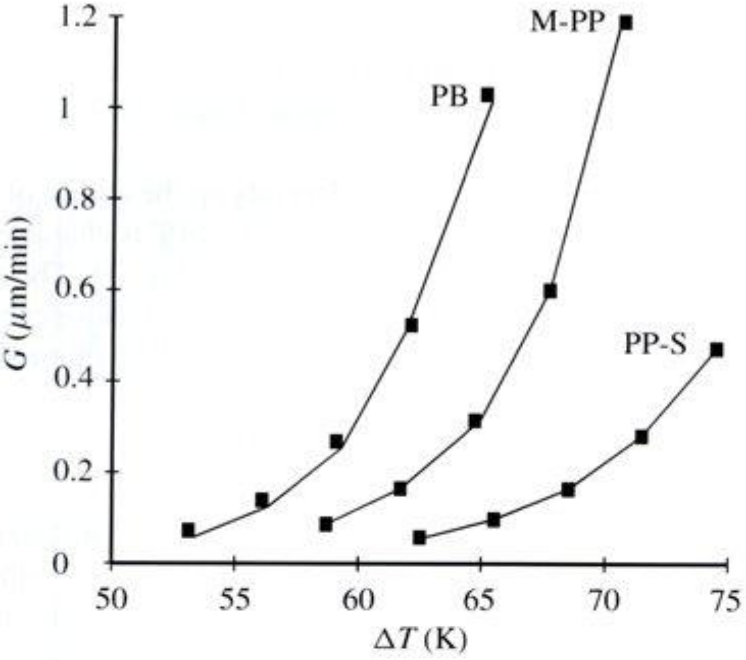

Figure 6. Dependence of the spherulite growth rate G on ΔT.

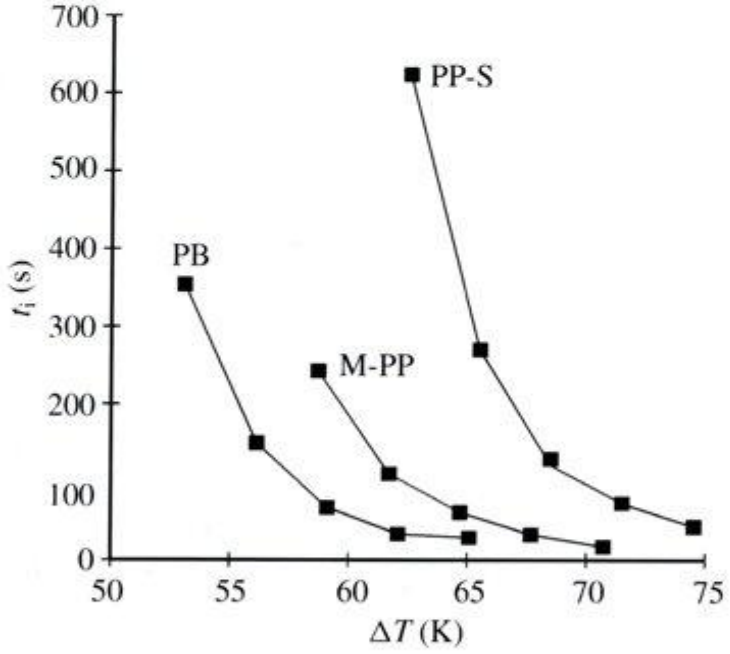

Figure 7. Dependence of the induction time on ΔT.

the half-time of crystallization versus supercooling, $\Delta T = T_m^o - T_c$ (Fig. 4): the crystallization of PB proceeds faster than that of PP-S, and the plot of M-PP lies between those of PP-S and PB. The same conclusion can be derived from Fig. 5, where the conversion curves for the PPs are presented for the same supercooling, $\Delta T = 65$ K.

Based on the relation for the spherulite growth rate, G, versus temperature, ΔT, obtained from our optical microscopy data [20] (Fig. 6), the values for growth rates

at given temperatures, investigated in this work by DSC, were calculated. The results obtained by DSC analysis were confirmed by microscopic investigation, since the highest lamella growth rate was again found for PB, while the lowest value was determined for pure PP.

The induction time for crystallization (t_i) depends on the ability of the polymer to undergo primary nucleation. Obviously, MAH-grafted PP is characterized by better conditions for nucleation compared with pure PP (see Fig. 7). The presence of the carbonyl groups of MAH in PP is believed to promote heterogeneous nucleation [15, 34, 35], and shorter induction times for both PB and M-PP might be attributed to this effect.

4.2. Nonisothermal crystallization

The study of nonisothermal crystallization of iPP is of significant technological importance, since most thermoplastic polymers and composites with thermoplastic matrices are processed under nonisothermal conditions. Furthermore, it is generally accepted that the rate of crystallization is of primary importance in polymer processing.

It is well known that due to the presence of nucleating agents, nonisothermal crystallization of nucleated polymers starts at a higher temperature [36]. In other words, the difference between T_m^o and the peak temperature of crystallization (the temperature at which the nonisothermal crystallization curve reaches its maximum), T_p, $\Delta T_p = T_m^o - T_p$, decreases as heterogeneous nucleation tends to increase. This effect becomes more significant as the cooling rate during crystallization becomes close to or lower than 3 K/min [37]. Using the data from DSC cooling runs, a formalism [38, 39] was developed for calculating the activity of substrates in the catalyzed nucleation of polymer melts.

The results obtained for the ΔT_p dependence on the cooling rate are shown in Fig. 8. It is seen that the ΔT_p difference is lowest for MAH-grafted PP and that the curve for M-PP lies between those for PB and PP-S. This implies that the possibility of heterogeneous nucleation is highest (or most pronounced) for PB and the addition of a small amount of this polymer containing maleic anhydride to iPP can affect its nucleation ability considerably. In the β range investigated (1–20 K/min), the nucleation ability of the modified polymer (M-PP) is improved compared with pure iPP. According to the data presented in Fig. 9 for the dependence of the peak crystallization temperature T_p on β, the same conclusion can be drawn: the crystallization of M-PP starts at the highest temerature, even higher than the crystallization temperature of PB. The onset crystallization temperature, $T_{c,o}$, determined for $\beta = 20$ K/min was 111°C for PP-S, 113°C for PB, and 119°C for M-PP (for $\beta = 3$ K/min: $T_{c,o} = 120$°C, 123°C, and 126°C, respectively).

Generally, the rate of crystallization depends on supercooling, which is a driving force for crystallization; additionally, in nonisothermal crystallization heterogeneous nucleation is of great importance, influencing the onset of crystallization and the temperature at which the maximum crystallization rate is reached. Despite the

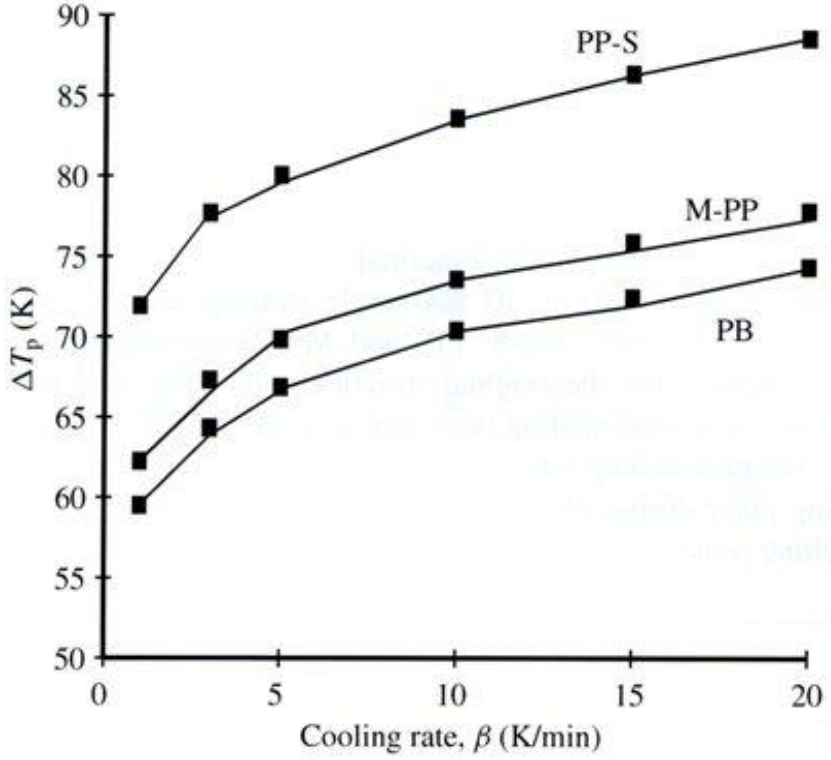

Figure 8. Dependence of ΔT_p on the cooling rate β.

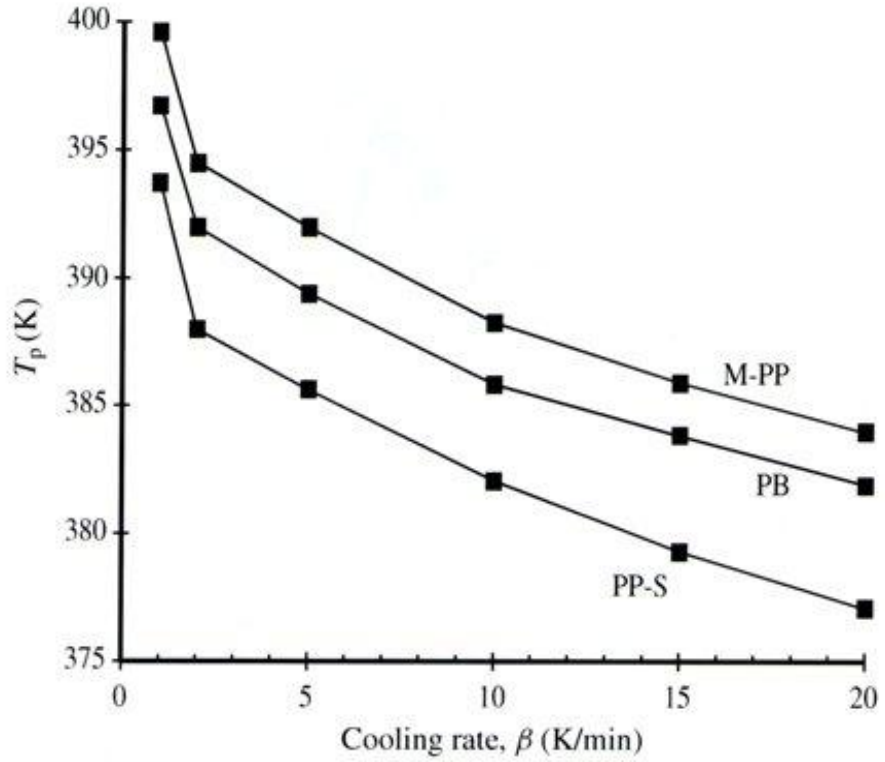

Figure 9. Dependence of T_p on the cooling rate β.

fact that T_m^o of PP-S is the highest, during crystallization from the melt it crystallizes at the lowest T_p, probably due to a depressed ability for heterogeneous nucleation. The crystallization of M-PP, although having weaker nucleating properties than PB, starts at a higher temperature (T_m^o of M-PP is higher than T_m^o of PB).

4.3. Melting behavior

The DSC melting curves of nonisothermally crystallized samples at different cooling rates are shown in Fig. 10. A single melting peak is observed on the thermograms of all samples (PP-S, PB, and M-PP) crystallized at low cooling rates. This indicates that the original structures are stable and not disposed to recrystallization. A second melting peak appeared on the thermograms of polymers crystallized at higher cooling rates ($\beta > 3$ K/min) as a result of a recrystallization process taking place during the heating run. To determine the temperature of low and high melting peaks, curve fitting was performed applying a normal log-function.

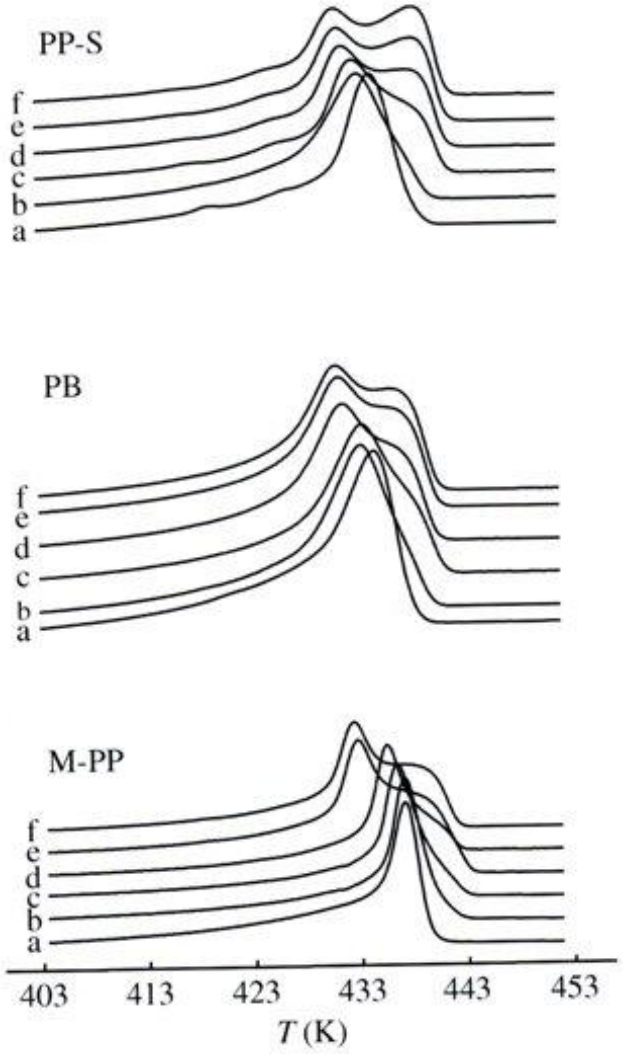

Figure 10. Heating thermograms ($\beta = 10$ K/min) of polymers crystallized at different cooling rates ($-\beta$ K/min): (a) 1; (b) 3; (c) 5; (d) 10; (e) 15; (f) 20.

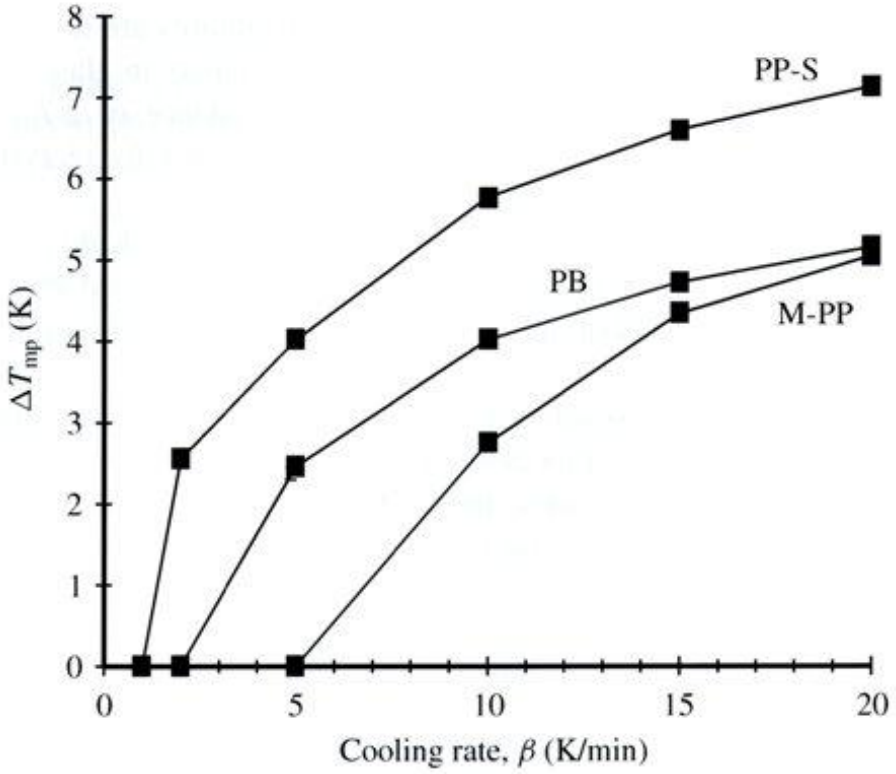

Figure 11. Difference between the temperatures of high (T_{hm}) and low melting (T_{lm}) peaks, ΔT_{mp}, versus the cooling rate β.

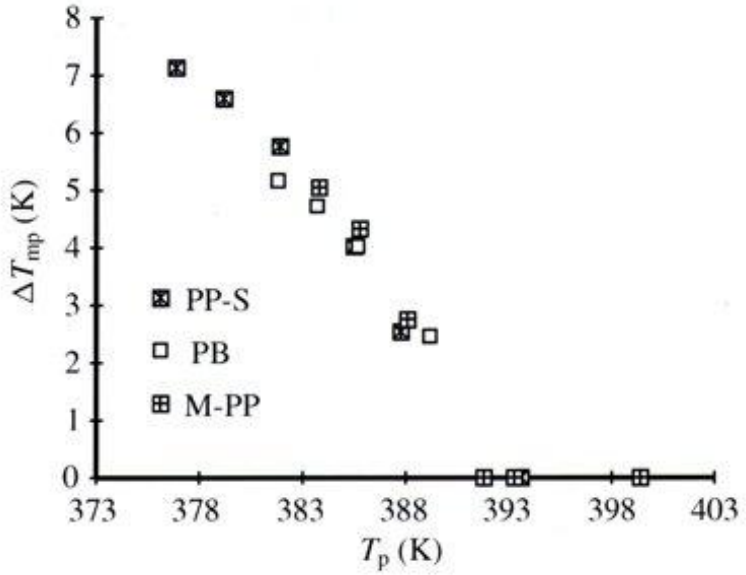

Figure 12. Difference between the temperatures of high (T_{hm}) and low melting (T_{lm}) peaks, ΔT_{mp}, versus T_p.

The difference between the high (T_{hm}) and low (T_{lm}) melting peaks, $\Delta T_{mp} = T_{hm} - T_{lm}$, is plotted against the cooling rate in Fig. 11. If this difference is accepted as a measure of the tendency for recrystallization during the DSC run, then from these results it becomes obvious that M-PP exhibits a stable crystalline structure, while homo-PP undergoes significant recrystallization. The crystalline structures

of polymers originating at higher crystallization temperatures are less disposed to recrystallization, as was shown for the investigated polymers in glass fiber model composites in our previous work [17, 18]. The dependence of ΔT_{mp} on T_p is presented in Fig. 12, and it can be observed that the tendency for recrystallization decreases with increasing peak temperature of crystallization.

The original crystal structures of polymers with T_p's over 390 K do not recrystallize. As a result, among the PPs investigated, the modified one (M-PP) exhibits a structure that is more stable than those of PB and PP-S, the latter two being most disposed to recrystallization.

Keeping in mind that the properties of semicrystalline polymers are related to the morphology developed during processing [heating (melting)/cooling (crystallization)], it is clear that besides the finest morphology [20], the crystallization behavior makes M-PP more appropriate for use in composite materials.

4.4. 'Fundamental' and 'practical' adhesion

The influence of the adhesion and/or the interphase between glass fibers and the investigated PPs on the micromechanical properties was evaluated by the pull-out test and the results are given in Table 4.

As confirmed by the pull-out test, the apparent shear strength, τ_{app}, of M-PP increased drastically. This is indirect proof for increased adhesion between the matrix and the fiber for the same sizing used. Although the determination of the apparent shear strength includes the interfacial adhesion at the interface, it seems to be a more reliable means of characterizing 'practical' adhesion [40].

The determination of the work of adhesion, W_A, by wetting of solid surfaces of PP-S and M-PP and sized glass plates by model liquids showed only small differences, which cannot explain the large difference in mechanical performance. Possible explanations are either the low sensitivity of wetting methods to local covalent bonds or the build-up of an interphase responsible for the changes in the mechanical properties, which could be due to the different crystallization behaviors and the appearance of transcrystalline zones (mechanical keying effect). This is a subject of our further investigations.

Table 4.
Comparison of single-fiber pull-out data and work of adhesion determined using the geometric mean in the Owens–Wendt approach

Sample	τ_{app} (MPa)	W_A (mJ/m^2)
PP-S	7.2	44.4
M-PP	15.8	47.8

5. CONCLUSION

The crystallization behavior of iPP was significantly altered by modification with a small amount MAH-grafted PP. The presence of MAH in the modified iPP decreases the equilibrium melting temperature and surface energy of folding, thus improving the conditions for secondary nucleation. As a consequence, the rate of crystal conversion was increased compared with neat iPP. The heterogeneous nucleation of MAH-modified iPP was also promoted. Better nucleation properties of the modified iPP were shown to cause a shift in the crystallization peak temperature towards higher values, resulting in original crystal structures less disposed to recrystallization. The apparent shear strength of single-fiber model composites with MAH-modified PP was significantly increased compared with homo-iPP. However, additional studies are needed to evaluate the influence of both fiber sizings and PP modifiers on the crystallization behavior in glass fiber composites.

Acknowledgements

The results presented in this paper are part of a bilateral project on thermoplastic-based fiber-reinforced composites between the Faculty of Technology and Metallurgy in Skopje and the Institute of Polymer Research Dresden, funded by the Ministry of Science of Macedonia and the International Bureau of BMBF, Germany. We are grateful to Dr. H. Komber for his help in NMR experiments. Dr. G. Pompe is gratefully acknowledged for useful suggestions regarding the text.

REFERENCES

1. P. L. Fernando, *Polym. Eng. Sci.* **28**, 806 (1988).
2. A. K. Gupta, K. R. Srinivasan and P. K. Kumar, *J. Appl. Polym. Sci.* **43**, 451 (1991).
3. B. Fillon, B. Lotz, A. Thierry and J. C. Wittmann, *J. Polym. Sci. Polym. Phys. Edn* **31**, 1395 (1993).
4. J. I. Velasco, J. A. Desaja and A. B. Martinez, *J. Appl. Polym. Sci.* **61**, 125 (1996).
5. D. H. Lee and K. B. Yoon, *J. Appl. Polym. Sci.* **54**, 1507 (1994).
6. H. N. Beck and H. D. Ledbetter, *J. Appl. Polym. Sci.* **9**, 2131 (1965).
7. K. Mitshuishi, S. Ueno, S. Kadawa and S. Kawasaki, *J. Appl. Polym. Sci.* **43**, 2043 (1991).
8. S. C. Tjong and S. A. Xu, *Polym. Int.* **44**, 95 (1997).
9. S. Vleshouvers, *Polymer* **38**, 3213 (1997).
10. J. Varga, *J. Mater. Sci.* **27**, 2557 (1992).
11. S. C. Tjong, J. S. Shen and R. K. Y. Li, *Polymer* **37**, 2309 (1996).
12. M. Davenport, *Reinforced Plastics* **40**, 26 (1996).
13. Q. Zheng, R. J. Morgan and R. Allred, *Polym. Prepr.* **36**, 777 (1995).
14. R. P. Singh, *Prog. Polym. Sci.* **17**, 251 (1992).
15. S. N. Sathe, G. S. S. Rao and S. Devi, *J. Appl. Polym. Sci.* **53**, 239 (1994).
16. A. R. Oromehie, S. A. Hashemi, I. G. Meldrum and D. N. Waters, *Polym. Int.* **42**, 117 (1997).
17. A. Janevski and G. Bogoeva-Gaceva, *J. Appl. Polym. Sci.* **69**, 381 (1998).
18. A. Janevski, G. Bogoeva-Gaceva and E. Mäder, *J. Appl. Polym. Sci.* (in press).
19. E. Mäder, H.-J. Jacobasch, K. Grudke and T. Gietzelt, *Composites* **A27**, 907 (1996).
20. G. Bogoeva-Gaceva, B. Mangovska and E. Mäder, *J. Appl. Polym. Sci.* (in press).

21. Y. Long, R. A. Shangs and Z. H. Stachurski, *Prog. Polym. Sci.* **20**, 651 (1995).
22. J. D. Hoffman, *Soc. Plast. Eng. Trans.* **4**, 315 (1964).
23. J. D. Hoffman, G. T. Davis and S. I. Lauritzen, in: *Treatise on Solid State Chemistry*, N. B. Hannay (Ed.), Vol. 3, pp. 497–614. Plenum Press, New York (1976).
24. H. L. Williams, R. F. Landel and J. D. S. Ferry, *J. Am. Chem. Soc.* **77**, 3701 (1955).
25. L. Grispino, E. Martuscelli and M. Pracella, *J. Macromol. Chem.* **181**, 1747 (1980).
26. S. Brandup and E. H. Imergut (Eds), *Polymer Handbook*, Vol. 5, p. 24. Interscience, New York (1975).
27. D. R. Gree and T. P. Melia, *Makromol. Chem.* **132**, 195 (1970).
28. J. J. Lauritzen and J. D. Hoffman, *J. Res. Natl Bur. Stand., Sect. A* **66**, 13 (1962).
29. M. J. Avrami, *Chem. Phys.* **7**, 1103 (1939).
30. M. J. Avrami, *Chem. Phys.* **9**, 177 (1941).
31. M. Avella, E. Martuscelli and M. Pracella, *J. Thermal Anal.* **28**, 237 (1983).
32. H. S. Bu, S. Z. D. Cheng and B. Wunderlich, *Macromol. Chem. Rapid Commun.* **9**, 76 (1988).
33. B. Monasse and J. M. Haudin, *Colloid Polym. Sci.* **263**, 822 (1985).
34. Z. Yin, Y. Zhang, X. Zhang and J. Yin, *J. Appl. Polym. Sci.* **63**, 365 (1997).
35. F. Rybnikar, C. Pospisil and J. J. Jankar, *Mater. Sci. Lett.* **9**, 499 (1990).
36. J. Varga, in: *Polypropylene, Structure, Blends and Composites*, J. Karger-Kocsis (Ed.), Vol. VI, p. 65. Chapman & Hall, Weinheim (1995).
37. R. Philips, J. Anders and J. A. Manson, *J. Polym. Sci. B: Polym. Phys.* **35**, 875 (1997).
38. A. Dobreva and I. Gutzov, *Cryst. Res. Technol.* **25**, 927 (1990).
39. A. Dobreva, A. Stoyanov and I. Gutzov, *J. Appl. Polym. Sci. Appl. Polym. Symp.* **48**, 473 (1991).
40. E. Mäder, K. Mai and M. Mühle, *Composite Interfaces* (in press).